

## STEPS TOWARD THE HUBBLE CONSTANT. I. CALIBRATION OF THE LINEAR SIZES OF EXTRAGALACTIC H II REGIONS

ALLAN SANDAGE AND G. A. TAMMANN\*

Hale Observatories, Carnegie Institution of Washington, California Institute of Technology

Received 1973 October 10; revised 1974 January 7

### ABSTRACT

Measurements of the angular sizes of the core and halo parts of H II regions are given for 11 galaxies in the Local and M81-NGC 2403 groups whose distances are known from Cepheid variables. Corrections for dependences on the experimental conditions are made by precepts developed in the Appendix. The apparent angular sizes are only weakly dependent on exposure time of the plates, showing that the measured sizes are defined essentially by conditions in the nebulae rather than by the observational techniques.

The linear dimensions of H II regions in the calibrating galaxies and in six galaxies of the M101 group [with  $(m - M)_0 = 29.3$  from Paper III of this series] increase steeply with the luminosity of the parent galaxies at a rate  $\Delta \log D / \Delta M_{pg} = -0.14$ . This is close enough to the distance-independent value of  $-0.2$  that straightforward use of H II diameters as distance indicators is impossible. Because of this  $D = f(M_{pg})$  dependence, nearby dwarf galaxies have nearly the same angular size for their H II regions as distant giant Sc galaxies of the same apparent magnitude.

To circumvent the difficulty, we have calibrated the linear diameters versus the *luminosity class* of the parent galaxy. The final correlation is tight, giving a 1-sigma spread of  $\sigma(\Delta D/D) = 0.06$  (6 percent) for the first-ranked halo diameters in Sc I galaxies, increasing to  $\sigma(\Delta D/D) = 0.24$  for luminosity class V Ir systems.

The mean size of the largest H II region (core plus halo diameters) is 550 pc for Sc I galaxies, decreasing to 110 pc for luminosity class V galaxies.

This is the first of a series of papers on successive steps for measurement of the Hubble expansion rate. This calibration of H II regions forms the basis for distances to general field galaxies (Paper IV), which itself is an intermediate step for distances to Sc I galaxies that are distant enough ( $cz \geq 4000 \text{ km s}^{-1}$ ) to permit reliable determination of the Hubble constant (Papers V and VI).

*Subject headings:* galaxies — nebulae — redshifts

### I. INTRODUCTION

Two fundamental numbers of observational cosmology are the Hubble expansion rate  $H_0 \equiv \dot{R}_0/R_0$ , and the deceleration parameter  $q_0 \equiv -\ddot{R}_0/R_0 H_0^2$ , both for the present epoch. Of the two, the Hubble rate<sup>1</sup> is extraordinarily difficult to measure directly because distances must be determined with high precision to galaxies that are so remote as to have significant expansion velocities. Cepheids have long since faded below plate limit for such galaxies.

The redshifts must be large enough so that the effect of mean random virial motions, or of any local velocity perturbation, can be neglected.

The error, if caused by random motions, can, of course, be reduced by using many galaxies at given distances, but only if the peculiar motions are truly

random. A systematic error will not be reduced by using a number of galaxies if the perturbations themselves are systematic, as de Vaucouleurs (1958, 1966) has often suggested.

To avoid the question of a local anisotropy altogether, leaving open the question of its existence, we choose to determine the Hubble constant using galaxies with expansion velocities greater than  $\sim 4000 \text{ km s}^{-1}$ . This requires new calibration of precision distance indicators that are brighter than Cepheids and that enable us to reach these distances.<sup>2</sup> Much of the work discussed in this series of papers concerns the isolation and calibration of such indicators.

Figure 1 summarizes the progressive outward distance intervals that must be breached in turn by different indicators, until the remote distances are

\* Permanent address: Astronomisches Institut der Universität Basel, Binningen, Switzerland. Temporary address: Hamburger Sternwarte, Hamburg 80, Germany.

<sup>1</sup> The rate  $H_0 \equiv \dot{R}_0/R_0 = cz/D$  is, naturally, a decreasing function of time because the distance  $D$  to any particular galaxy increases due to the expansion. Furthermore, in the presence of deceleration, the redshift  $cz$  decreases as well. [Explicit expressions for  $H(t)$  as a function of  $q_0$  are derived elsewhere (Sandage 1961, 1962a).] Nevertheless, in this series of papers the expansion rate will be called the Hubble constant, as we need consider only data at the present epoch because the light travel time to all galaxies involved in the present material is negligible compared with the time  $H_0^{-1}$ .

<sup>2</sup> It is known from the data on clusters of galaxies (Sandage, Tammann, and Hardy 1972, fig. 1; Sandage 1972, figs. 2-4; Sandage and Hardy 1973, fig. 7) that no large perturbations exist in the velocity field for redshifts larger than about  $4000 \text{ km s}^{-1}$ . The evidence comes from the lack of systematic deviation of the clusters from the theoretical Hubble line of slope 5 as  $m \propto 5 \log cz$ . The data show that the value of  $H_0$  determined in the range  $3000 \lesssim cz \lesssim 10,000 \text{ km s}^{-1}$  will require no correction to convert it to a value with global significance, contrary to the conclusion of Haggerty and Wertz (1972). Justification from this point of view is given elsewhere (Sandage *et al.* 1972).

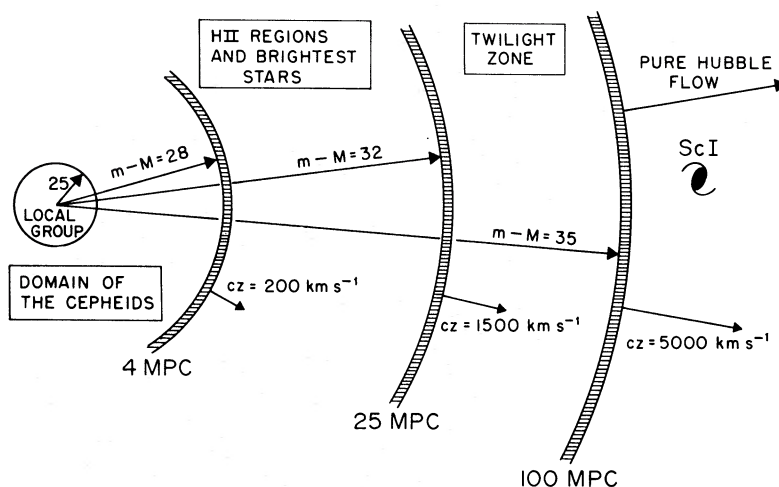


FIG. 1.—Schematic representation of distance intervals within which various components of the stellar content of late-type galaxies are resolved to a working plate limit of  $m_{pg} \approx 22$ . Cepheids, H II regions, and brightest stars have generally become too small or too faint for routine measurement at distances greater than  $D \approx 25$  Mpc.

reached where a pure Hubble flow is known to exist.<sup>3</sup> The first distance interval ( $m - M \approx 25$ ;  $D \approx 1$  Mpc) contains the Local Group of galaxies. Cepheid variables are found here and in the next interval to  $m - M \approx 28$ , which embraces the M81–NGC 2403 group (Holmberg 1950; Tammann and Sandage 1968) and the South Polar Group (de Vaucouleurs 1959). The systematic expansion velocity at this distance is only  $cz \approx 200$  km s<sup>-1</sup>. The Hubble constant cannot be well determined by using such nearby galaxies.

Individual distance indicators, such as brightest blue stars ( $M_B \approx -10$ ) and the size of H II regions, can be detected in late-type giant spiral galaxies to moduli as large as  $m - M \approx 32$ . The apparent magnitude of such stars is  $B \approx 22$ , and the angular size of the largest H II region ( $D \approx 400$  pc derived later) is  $3''$ ; both indicators are then just above plate limit routinely. But even at this distance the expansion velocity is less than  $1500$  km s<sup>-1</sup> (if  $H_0 \approx 50$  km s<sup>-1</sup> Mpc<sup>-1</sup> as derived later), which again is too small.

There is then a twilight zone between  $m - M \approx 32$  (where the last distance indicators, aside from supernovae, have disappeared), and  $m - M = 35$  where there is evidence that a pure Hubble flow exists ( $cz \approx 5000$  km s<sup>-1</sup>). It is beyond this region that the calibration for  $H_0$  must be made. This gap is bridged in the present work by the following series of steps.

1. The linear sizes of H II regions in late-type spirals (Sc–Sd–Sm) and Ir galaxies are calibrated using galaxies whose distances are known from Cepheids ( $m - M \lesssim 28$ ) (this paper).

2. This size calibration is extended to include super-

giant spirals. The distance to the nearest of these (M101) is found in Paper III using six methods, including use of the brightest stars as calibrated in Paper II.

3. The H II region sizes are used to determine distances to 50 late-type field galaxies in the distance interval  $m - M < 32$  (Paper IV). The *distribution of absolute magnitudes* of the galaxies in this 50-galaxy sample, as a function of luminosity class (Paper IV), follows from these data.

4. Redshifts of newly identified giant Sc I spirals with  $m - M > 35$  have been measured as the last step. Combining the redshifts and the absolute magnitudes of step 3 gives  $H_0$ . Because this value is independent of the redshifts for galaxies closer than  $m - M = 35$  (Paper VI), the local velocity field does not enter the problem. Any supposed perturbation of the local kinematic field is a separate issue (cf. Paper V) that does not affect the value of  $H_0$  determined in this way.

Our final value of the expansion rate differs by a factor of 10 from the distance scale of Hubble and Humason (1931) and of Hubble (1936a, b, c). Baade (1952, 1956) changed Hubble's scale *within the Local Group* by a factor of 2 from his recalibration of the Cepheid luminosities. An additional factor of 5 for more distant galaxies arises from several causes that include (1) corrections of faint magnitudes (Stebbins, Whitford, and Johnson 1950; Purgathofer 1969; Baum, unpublished) for scale errors in the Seares, Kapteyn, and van Rhijn (1930) magnitudes, universally used as standards throughout the 1930s; (2) separation of stars from H II regions in nearby galaxies using red sensitive plates (Humason, Mayall, and Sandage 1956; Sandage 1958); and (3) change in the absolute magnitudes of the brightest stars from  $\langle M_B \rangle \approx -6$  (Hubble 1936a) to  $\langle M_B \rangle \approx -10$  here (Paper II). A preliminary discussion of these factors some time ago (Sandage 1958) led to  $H_0 = 75$  km s<sup>-1</sup> Mpc, but the new data discussed in this series supersede both this

<sup>3</sup> Such a flow may exist at smaller distances as well, but our detailed mapping of the kinematic field for distances less than 10 Mpc ( $m - M = 30$ ) is not yet complete or accurate enough to independently test for the presence or absence of a local anisotropy as discussed by de Vaucouleurs. The extent to which our present data can be used for such a test will be discussed in Paper V of this series (Sandage and Tammann 1974).

TABLE 1  
COMPARISON OF HUBBLE'S DISTANCES WITH NEW FINAL  
VALUES HERE FOR SELECTED GALAXIES

Object	$(m - M)_{\text{Hubble}}^{\text{AB}}$	$(m - M)_{\text{Here}}^{\text{AB}}$	Scale Factor
M31.....	22.0	24.84	3.7
NGC 2403...	24.0	27.56	5.2
M101.....	23.5	29.3	14.4
Virgo cluster.	26.8	31.4	8.3

early report and an interim discussion of a *lower limit* to the distance of the Virgo cluster (Sandage 1968).

The change that has been made here in Hubble's distance scale is not a constant, but is a progressive factor that increases with distance until  $(m - M)_{\text{new}} \simeq 32$  is reached. The stretch factor is listed in table 1, where our present distances are compared with those of Hubble for particular galaxies. Here,  $(m - M)_{\text{AB}}$  is the apparent modulus in the *B* passband. The ratio of our distance to Hubble's scale is listed in the last column. The scale factor within the Local Group is  $\sim 3.7$ ; it increases to 5 at the M81 group, and to  $\sim 10$  at the Virgo cluster, beyond which it remains constant. It is a constant factor beyond Virgo because the earlier data (Hubble and Humason 1931, fig. 5) and the later material (Sandage 1972, fig. 2) both have a slope of 5 in the redshift-magnitude relation for all clusters beyond Virgo, which means that the *ratio* of cluster distances is the same in both studies.

The present paper describes the calibration of H II region linear sizes as a function of galaxy absolute magnitude (step 1).

## II. THE DATA

We have restricted the present study to late-type galaxies of class Sc, Sd, Sm, and Ir, neglecting the Sa and Sb types. Sa galaxies have few if any H II regions, presumably because of the absence of many hot early-type stars. Similarly Hodge (1966) could show that Sb galaxies generally have fewer H II regions than Sc's of the same total luminosity. In addition, Sersic (1960) in his pioneering study showed that the linear sizes of H II regions in Sa and Sb systems were systematically smaller than in Sc's. The diameter-type relation peaked broadly near Sc<sup>-</sup> (Sersic 1960, table 2a), declining on either side in Sersic's material.

We eliminate Sa and Sb from our present sample because of this type-size relation, but include Scd, Sd, Sm, and Ir systems and show that in this combined grouping, the linear size of the first three largest H II regions is a strong, tight function of absolute galaxy magnitude. Sersic's decline in linear size for his Sc, Ir I, and dSc groups may be a result of this absolute-magnitude dependence, rather than a multiple dependence on galaxy type and on luminosity as in Sb and Sc's.

The observations were begun in 1954 using red plates (Eastman 103aE) behind an RG1 or an RG2 broad-band filter. An intermediate-band (80 Å total half-width) H $\alpha$  interference filter was used after 1959. This filter, with 103aE plates, required 2-hour expo-

sure at the prime focus of the Hale reflector (*f*/3.67) for adequate plate density. Only nights of good to excellent seeing were used, and the observational program proceeded slowly, extending over 19 years.

Adequate plate material for steps 1 and 3 of the problem was available only after 1969 when the last phases of the program were finished using an electrostatic S20-type image-tube behind the H $\alpha$  filter, giving an effective gain of  $\sim 10$  over the unaided plate.

Plate material exists for galaxies in the Local Group, the M81 group, the M101 group, and about 40 galaxies in the general field of the northern hemisphere. The distribution among the luminosity classes (van den Bergh 1960a) is 10 Sc I, three Sc I-II, six Sc II, three Sc II-III, four Sc III and Ir III, six Sc III-IV and Ir III-IV, seven Sc IV and Ir IV, one Ir IV-V, six Sc IV-V and Ir IV-V, and two Ir V.

### a) The Calibrating Galaxies

There are 11 galaxies in the sample whose distances are known from Cepheids. These are LMC, SMC, M33, NGC 6822, and IC 1613 in the Local Group, and NGC 2403, NGC 2366, NGC 4236, IC 2574, Ho I, and Ho II of the M81-NGC 2403 group. We have adopted the distances of the M81-NGC 2403 group members to be that of NGC 2403, as measured earlier in a study that was preliminary to the present problem (Tammann and Sandage 1968). The assumption is justified in § V of the forthcoming Paper II in this series.

The data for the 11 calibrating galaxies are set out in table 2. Listed are the galaxy types, luminosity classes, adopted blue galactic absorptions  $A_B$ , distance moduli, and apparent and absolute magnitudes. The sources for these data are given in the last column by numbers that are identified in footnotes to the table.

The brighter and largest H II regions in 11 galaxies were identified, and the three largest were chosen for measurement in each galaxy (§ IIb). The regions are marked in figures 2-8 (plates 8-14) for all the calibrating galaxies with the exception of LMC and IC 1613 where adequate marked photographs already exist in the literature (Henize 1956; Sandage 1971).

### b) Definition of Angular Diameter

H II regions are generally irregular in shape, and sometimes have ill-defined boundaries. To include all types of H II regions, and to obtain data that are as far as possible free of systematic error with distance, we experimented with various operational definitions of diameter.

On the large-scale plates, many H II regions generally appear to be composed of two regions, a core and a halo. The border of the *core* is normally well defined, and there is little uncertainty as to what should be measured for the core boundary. We suspect that the intensity profile across the H II region is, in fact, continuous, and that what appears as the "core" to the eye may be but a change in the intensity gradient. Nevertheless, the core is well defined for visual measurement, and the "core diameter" so measured

TABLE 2  
BASIC DATA FOR THE 11 CALIBRATING GALAXIES IN THE LOCAL GROUP AND THE M81 GROUP

Galaxy	Type	$L_C$	$(m - M)_{AB}$	$b^{II}$	$A_B$	$(m - M)_0$	$m_{pg}$	$M_{pg}^0$	$r$ (kpc)	Sources
LMC.....	Ir to SBc	III-IV	18.91	-44°	0.32	18.59	1.05	-17.86	52.2	1, 2, 3, 4
SMC.....	Ir	IV to IV-V	19.35	-33	0.08	19.27	2.93	-16.42	71.4	1, 2, 3, 4
M33.....	Sc	II-III	24.68	-31	0.12	24.56	6.19	-18.49	81.7	5, 6, 7, 8
NGC 6822.....	Ir	IV-V	25.03	-18	1.08	23.95	9.21	-15.82	616	5, 9, 10, 8
IC 1613.....	Ir	V	24.55	-61	0.12	24.43	10.00	-14.55	769	11, 12, 8
NGC 2403.....	Sc	III	27.80	29	0.24	27.56	8.80	-19.00	3250	5, 13, 8
NGC 2366.....	S <sup>+</sup> or Ir <sup>+</sup>	IV-V	27.75	29	0.19	27.56	11.41	-16.34	3250	5, 13, 14, 8
NGC 4236.....	SB <sup>+</sup> or Ir <sup>+</sup>	IV	27.58	47	0.02	27.56	10.05	-17.53	3250	5, 13, 14, 8
IC 2574.....	S	IV-V	27.60	44	0.04	27.56	10.91	-16.69	3250	11, 13, 14, 8
Ho II.....	Ir	IV-V	27.67	33	0.11	27.56	11.14	-16.53	3250	11, 13, 14, 8
Ho I.....	Ir	V	27.63	39	0.07	27.56	13.27	-14.36	3250	11, 13, 14, 8

SOURCES.—(1) van den Bergh 1960*b*. (2) Sandage and Tammann 1971. (3) Gascoigne 1969. (4) de Vaucouleurs and de Vaucouleurs 1964: The  $B(0)$  magnitudes from this source are transformed into Holmberg's (1950)  $m_{pg}$  system by  $m_{pg} = B(0) + 0.149(B - V) - 0.22$ . (5) van den Bergh 1960*c*. (6) Sandage 1962*b*. (7) McClure and Racine 1970. (8) Holmberg 1957. (9) Kayser 1967. (10) Tammann 1969. (11) van den Bergh 1966. (12) Sandage 1971. (13) Tammann and Sandage 1968. (14) The absorption  $A_B$  is calculated from a modified cosecant law of  $A_B = 0.132(\csc b - 1)$  from Sandage 1973.

has proved to be a stable statistic (§ IIc and the Appendix).

The boundary of the halo is defined as the outer border traceable by visual inspection on a given plate. Surprisingly, in our material this boundary proved to be only weakly dependent, if at all, on exposure time (§ III and the Appendix), which suggests that the brighter and largest H II regions are radiation bounded, rather than density limited (Strömgren 1939). A rather sharp outer boundary to H II regions exists in the former case at the place where hydrogen changes mostly from H II to H I due to the dilution effect on the radiation field as we move outward from the exciting star(s). In this transition zone, the optical depth to the ionizing radiation from the central source shortward of  $\lambda 912 \text{ \AA}$  becomes very large, the emission measure decreases abruptly, and the H II region is sharply bounded at that place, which we take to be our halo boundary. No such boundary exists in the density-limited case where the entire H II region is transparent to the source radiation (i.e., the available number of hydrogen atoms is too small for the nebula to extend into the transition zone; and the diameter, which is now ill defined, depends in detail on the available hydrogen density and its decline with radial distance).

The angular diameter we have adopted is the mean of four dimensions: the major and minor diameters of the halo and the core. Some H II regions have no core (those of low surface brightness, and those of the ring type [Gum and de Vaucouleurs 1953]), and the core diameters have been assigned a value of zero for them.

In the late-type galaxies of high surface brightness (e.g., NGC 2903, M51, NGC 5236, etc.), the blue light from the young population in the spiral arms confuses the separation and the measurement of the halo size of the embedded H II regions. This blue population is, of course, strongly suppressed on the red plates. The red plates have proved to be essential for the present problem for the aforementioned reasons.

In summary, we wish to emphasize that the H II regions we have marked are discrete structures, and not merely the peaks of fluctuations of a general continuous H $\alpha$  emission along spiral arms. We appreciate the point that H II halo diameters would have been impossible to define if this had not been the case (e.g., as implied in Carranza, Crillon, and Monet 1969). The conclusion from the near independence of our halo sizes with exposure time is that most of the brightest and largest H II regions measured here are indeed radiation bounded.

#### c) *Uncorrected Values of Angular Sizes for H II Regions in the Calibrating Galaxies*

The ranking of the H II regions within a galaxy was done on the basis of the mean of *all four measurements* (major and minor axes for core and halo) for each H II region. This procedure favors the conspicuous regions with large cores, and gives less weight to the extended, low surface brightness (coreless) regions. The procedure has the advantage that the very low surface brightness objects, whose detection will be distance dependent (the worst possible bias for the present problem), are largely suppressed from the data. The marked regions in figures 2-8 are generally of high surface brightness for these reasons.

The regions measured in the LMC, not illustrated here, are 30 Doradus (No. I), He 11 (II), and He 44 (III) as identified by Henize (1956); for IC 1613 the first three ranked are Baade 10, 15/16, and 3 (Sandage 1971, fig. 13).

The measurements were made by eye estimates using an eyepiece with 0.2-mm graduations. The sizes were read to 0.1 mm, or in certain well-defined cases to 0.05 mm.

Occasionally the outer borders of an H II region will embrace more than one core (for example, the H II complex in Orion). In these cases only the largest core was considered and measured. In other cases the definition of the outer boundary is ambiguous. For

TABLE 3  
RAW MEASUREMENTS OF THE ANGULAR SIZES OF THE FIRST THREE RANKED  
H II REGIONS IN THE CALIBRATING GALAXIES

Galaxy	Plate	Filter	Exposure	Seeing <sup>2)</sup>	$\alpha_{IH}$ (maj)	$\beta_{IH}$ (min)	$\alpha_{IC}$ (maj)	$\beta_{IC}$ (min)	$\alpha_{IIH}$ (maj)	$\beta_{IIH}$ (min)	$\alpha_{IIC}$ (maj)	$\beta_{IIC}$ (min)	$\alpha_{IIIH}$ (maj)	$\beta_{IIIH}$ (min)	$\alpha_{IIIC}$ (maj)	$\beta_{IIIC}$ (min)
LMC	Bex-164-H <sup>3)</sup>	Red Plexiglass	315		1970"	1640"	1040"	790"	1260"	1170"	300"	210"	1040"	630"	470"	160"
SMC	Bex-115-H <sup>3)</sup>	"	300		647	631	221	126	410	394	0	0	315	284	0	0
M33	PS-8115-S	H $\alpha$	180	1-3	144	104	71	53	125	118	64	40	158	140	15	12
	PS-8117-S	H $\alpha$	180	2-3	148	78	67	54	114	98	60	47	141	117	13	10
	PH-1095-S	RG1	99	3-4	105	80	49	31	91	49	24	16	...	...	...	...
NGC 6822	PH-403-B <sup>5)</sup>	GG1 + No25	80	3	44.2	39.8	15.5	11.1	53.1	50.9	0	0	28.8	22.1	16.6	8.8
	H-143-S	RG2	75	3-4	54.4	44.8	16.0	11.2	51.2	51.2	0	0	30.4	25.6	8.0	3.7
IC 1613	PH-814-B	RG2	68	3+	44.2	34.3	0	0	33.2	33.2	2.2	2.2	28.8	8.8	0	0
NGC 2403	PH-3901-S	H $\alpha$	145	3-1	44.2	28.8	14.4	12.2	39.8	23.2	8.8	6.6	24.3	15.5	7.7	4.4
	PH-257-S	RG1	35	2	44.2	28.8	15.5	13.3	35.4	22.1	6.6	4.4	28.8	16.6	8.8	3.3
	PH-564-B	RG2	60	2-3	...	...	...	...	35.4	22.1	6.6	5.5	28.8	15.5	8.8	3.3
	PH-726-S	RG2	90	3-4	37.6	33.2	16.6	12.2	33.2	26.5	6.6	10.0	28.8	22.1	11.1	8.8
	PH-570-B	RG2	120	3	44.2	33.2	14.4	12.2	33.2	24.3	8.8	7.7	28.8	22.1	10.0	8.8
	PH-575-B	RG2	120	3	43.1	29.9	15.5	13.3	33.2	24.3	11.1	10.0	26.5	22.1	13.3	10.0
NGC 2366	PH-4053-S	H $\alpha$	110	4	24.3	16.6	11.1	6.6	16.6	13.3	2.2	1.7	13.3	8.8	1.7	1.1
NGC 4236	PH-4522-S	H $\alpha$	120	3	39.8	16.6	8.8	5.5	27.7	17.7	4.4	2.2	25.4	17.7	4.4	3.3
IC 2574	PH-513-S	RG1	80	3	19.9	18.8	12.2	5.5	16.6	8.8	4.4	4.4	15.5	11.1	1.1	1.1
	PH-489-S	RG2	120	1-3	18.8	18.8	6.6	5.5	16.6	8.8	4.4	3.3	15.5	13.3	2.2	2.2
Ho II	PH-5151-Z <sup>7)</sup>	H $\alpha$	60	3-4	27.7	18.8	2.2	2.2	22.1	18.8	1.1	1.1	22.1	15.5	0	0
Ho I	PH-5742-S <sup>8)</sup>	H $\alpha$	15	3	22.1	13.3	2.2	2.2	15.5	13.3	2.2	1.1	8.8	7.7	1.1	0.6
	PH-5743-S <sup>8)</sup>	H $\alpha$	7	3	17.7	5.5	1.1	1.1	14.4	8.8	1.1	1.1	8.8	8.8	0	0

## Notes to Table 3

1. Bex = Mount Wilson 10" in South Africa; PS = 48" - Schmidt telescope, Palomar Mountain; H = 100" - Hooker telescope, Mt. Wilson; PH = 200" reflector, Palomar Mountain. The last letter designates the observer: H = Henize; S = Sandage; B = W. Baade; Z = H. Zirin.
2. Seeing 5, 3, and 1 corresponds to stellar seeing disks of 0".5, 1", and 3", respectively.
3. A contact glass copy of the original plate was used.
4. Off plate.
5. A paper copy of the original plate, never returned from loan, was used.
6. Near edge of plate.
7. Taken with an electrostatic image tube.
8. Taken with ITT image tube.

some types of regions, the outer borders exhibit regular patterns such as circular or oval disks, rings, S and horseshoe structures, and the shape can be regularized by an embracing ellipse. However, other H II regions are quite amorphous (e.g., 30 Dor in the LMC), and more personal judgment is required.

All measurements, made by one of us (G.T.), are listed in table 3. The Sc data together with similar data to be given in Paper IV (Sandage and Tammann 1974) form the basis of our system of H II region angular sizes. The linear calibration (§ V, fig. 9) rests on table 3 (as corrected to a standard plate type and exposure [§ III]), and on the distances of table 2. Other workers using the final calibration here (figs. 10 and 11) must first determine the correspondence of their personal system of measurement to that of table 3, before applying the present calibrations. The 21 plates of table 3 were taken with various filter types, telescopes,

emulsions, and detectors (image-tube or direct plates) as identified in the notes to the table.

### III. CORRECTIONS OF THE MEASUREMENTS TO STANDARD CONDITIONS

No corrections for seeing were made to the data because the seeing was better than 2" on nearly all of the plates; on many it was as good as 1". Most dimensions of the H II regions are considerably larger than 1", and the seeing effects are generally negligible on the present material.

To test if the measurements are strongly or only weakly dependent on the observational conditions, we purposely took the plates with different exposure times, and with different plate-type and filter combinations. Analysis of the data in table 3 is given in the Appendix for six possible instrumental dependences.

TABLE 4  
ANGULAR SIZES REDUCED TO STANDARD  
CONDITIONS BY EQUATIONS IN THE APPENDIX

		I		II		III		$\langle \theta \rangle_1$	$\langle \theta_H, \theta_C \rangle_1$	$\langle \theta \rangle_3$	$\langle \theta_H, \theta_C \rangle_3$
		$\theta(\text{maj})$	$\theta(\text{min})$	$\theta(\text{maj})$	$\theta(\text{min})$	$\theta(\text{maj})$	$\theta(\text{min})$				
LMC	halo	1970"	1640"	1260"	1170"	1040"	630"	1805"	1360"	1285"	890"
	core	1040	790	300	210	470	160	915		495	
SMC	halo	647	631	410	394	315	284	639	406	447	252
	core	221	126	0	0	0	0	174		57.8	
M33	halo	133	87	114	96	150	111	110	82.0	115	76.3
	core	62	46	54	38	14	11	54.0		37.5	
NGC 6822	halo	49.3	42.3	51.7	51.1	29.6	23.9	45.8	29.7	41.3	24.5
	core	15.8	11.2	0	0	12.3	6.3	13.5		7.60	
IC 1613	halo	44.2	34.3	33.2	33.2	28.8	8.8	39.3	19.6	30.4	15.6
	core	0	0	2.2	2.2	0	0	0.0		0.73	
NGC 2403	halo	38.6	27.8	31.6	21.4	24.8	17.0	33.2	22.2	26.9	17.4
	core	12.2	10.1	6.5	5.8	7.8	5.0	11.2		7.90	
NGC 2366	halo	24.3	16.6	16.6	13.3	13.3	8.8	20.5	14.7	15.5	9.78
	core	11.1	6.6	2.2	1.7	1.7	1.1	8.85		4.07	
NGC 4236	halo	39.8	16.6	27.7	17.7	25.4	17.7	28.2	17.7	24.2	14.5
	core	8.8	5.5	4.4	2.2	4.4	3.3	7.15		4.77	
IC 2574	halo	17.0	16.5	14.6	7.7	13.6	10.8	16.8	11.2	13.4	8.35
	core	7.1	4.1	3.3	2.9	1.3	1.3	5.60		3.33	
Ho II	halo	23.3	15.8	18.5	15.8	18.5	13.0	19.5	10.5	17.5	9.10
	core	1.5	1.5	0.7	0.7	0	0	1.50		0.73	
Ho I	halo	17.4	8.1	13.1	9.6	7.7	7.3	12.8	6.98	10.5	5.68
	core	1.2	1.2	1.2	0.8	0.4	0.2	1.20		0.83	

Most important is the effect of different exposure times on the apparent angular diameters. As previously mentioned (§ II), only a very weak dependence was found, ensuring that the corrections to a standard exposure ( $H\alpha$  interference filter plate of exposure 120 minutes with the f/3.67 focus at the Hale 200-inch [5-m] reflector) are small (any errors in the correction are therefore also small).

Effects due to bright background radiation (for the broad-band RG filter series), and to some properties of the transfer function of the image tube were found (Appendix, §§ IV, VI), and are moderately well determined.

Analysis of data measured on blue plates (Appendix, § VII) indicates that there are difficulties in measuring *core* diameters on broad-band blue plates, but that measurements of the halo sizes on blue plates are not excessively different from those obtained from the narrow-band red plates.

Equations (A1)–(A6) of the Appendix have been used to reduce all data in table 3 to the standard  $H\alpha$  exposure conditions. The reduced, adopted angular sizes of the core and halo parts of H II regions in the 11 calibrating galaxies are listed in table 4.

#### IV. ERRORS

The errors of entries in tables 3 and 4 are due to personal errors of measurement, and to differences between plates.

#### a) Measuring Error

The measurements for each H II region were repeated twice on each plate in such a way as to erase all memory of the first measurement. The measurements, averaged, are listed in table 3 without corrections. The differences  $\Delta\theta_i = \theta_i - \langle \theta \rangle$  provide a double set of deviations from the mean for repeated measurements on a given plate. The distribution of differences is closely Gaussian with  $\sigma(\Delta\theta/\langle \theta \rangle) = 0.065$  for a single measurement of halo dimensions, and  $\sigma(\Delta\theta/\langle \theta \rangle) = 0.184$  for single core measurements. One-sigma errors of each entry (mean of two measurements) in table 3 due to personal measuring error alone are therefore 5 percent for halo and 13 percent for core data.

#### b) Plate Error

However, random effects from plate to plate are larger than the measuring errors. More than one plate is available for eight galaxies in table 3 to show this. The data were reduced to standard conditions by the precepts in the Appendix; the mean  $\langle \theta \rangle$  were formed, and differences  $\Delta\theta_i = \theta_i - \langle \theta \rangle$  taken. Again the distribution of  $\Delta\theta/\langle \theta \rangle$  is closely Gaussian, with  $\sigma(\Delta\theta/\langle \theta \rangle) = 0.12$  for single halo measurements, and 0.24 for single core measurements.

The rms error in the adopted mean for the 11 galaxies in table 3 is, then, about  $\sqrt{2}$  smaller than these values because 21 plates could be measured for them.

Because the plate errors are about 1.5 to 2 times larger than the personal measuring errors, we conclude that our measuring procedure is adequate for the present material.

c) Total Random Error of Mean Diameters

Various combinations of the core and halo dimensions are used in the analysis of § V; each will have its characteristic random error according to how the mean diameter is formed.

The mean extensions of the core  $\langle \theta \rangle_C$  and halo  $\langle \theta \rangle_H$  themselves are, as mentioned, the average of the major and minor axes. Hence, the mean of the core plus halo  $\langle \theta_H, \theta_C \rangle \equiv \frac{1}{2}(\langle \theta \rangle_H + \langle \theta \rangle_C)$  is formed from four measurements. Clearly, the random error of  $\langle \theta_H, \theta_C \rangle$  is largely determined by the random error of  $\theta_H$  alone because the core measurements are, on the average, 3 times smaller than  $\theta_H$ .

The random errors of any given mean dimension depend, of course, on the number of independently determined quantities that go into the determination. The principal quantities we later use are defined in the summary table 5 together with their rms random errors calculated from the data in the last two sections.

V. THE CALIBRATION

The normalized angular measurements (table 4) were converted to linear sizes by using distances adopted from table 2, column (10), with the results listed in table 6. The linear diameters are clearly correlated with the absolute luminosity of the parent galaxy. The trend can be seen directly by inspection of figures 3-8 by noting the marked scale of the prints. The angular size of H II regions are smaller in the dwarf galaxies (Ho I, Ho II) than in NGC 2403, for example: Ho I is an extreme dwarf ( $M_{pg}^0 = -14.4$ ), while NGC 2403 is of intermediate luminosity class (III,  $M_{pg}^0 = -19.0$ ).

The range of luminosities among the 11 calibrators is but half the range available in nature, as there are no galaxies here brighter than class II-III (M33). Because it is crucial to extend the calibration to luminosity class I spirals, we made a major effort (Paper III) to determine the distance to the M101

TABLE 5  
SUMMARY OF MEASURING ERRORS FOR VARIOUS QUANTITIES

TYPE OF MEASUREMENT	SYMBOL	NUMBER OF MEASUREMENTS		RMS ERROR OF $\Delta\theta/\theta$
		Halo	Core	
Largest H II region:				
Halo.....	$\langle \theta_H \rangle_1$	2	0	0.06
Core.....	$\langle \theta_C \rangle_1$	0	2	0.12
Core + halo...	$\langle \theta_H, \theta_C \rangle_1$	2	2	0.05
Three largest H II regions:				
Halo.....	$\langle \theta_H \rangle_3$	6	0	0.035
Core.....	$\langle \theta_C \rangle_3$	0	6	0.07
Core + halo...	$\langle \theta_H, \theta_C \rangle_3$	6	6	0.03

group which is the nearest aggregate that contains an Sc I supergiant spiral. Six methods discussed in Paper III give  $(m - M)_0 = 29.3$  which permits all members of the group to be included in the calibration [one Sc I (M101); three Sc or Ir IV (NGC 5204, NGC 5474, NGC 5585); and two Irr IV-V (NGC 5477, Ho IV)].

a) Calibration as a Function of  $M_{pg}^0$

The result using the 17 calibrating galaxies is shown in figure 9. Plotted is the linear diameter (in parsecs) of the mean core plus halo diameters of the first three largest regions  $\langle D_H, D_C \rangle_3$  as a function of absolute magnitude of the parent galaxy. Open circles are the five galaxies in the Local Group; closed circles are the six galaxies in the M81-NGC 2403 group, and the crosses are the six systems of the M101 group. (Note the log scale of the ordinate.)

The formal least squares solution for the increase in H II size with absolute magnitude is

$$\log \langle D_H, D_C \rangle_3 = -0.140 M_{pg}^0 - 0.202, \quad (1)$$

with a dispersion, read at constant  $M_{pg}^0$ , of  $\sigma(\Delta \log D) = 0.09$ . (The solution was made with  $M_{pg}$  as independent variable because there is very little uncertainty in its value for the calibrating galaxies; their distances are presumably well known.)

The sense and magnitude of the increase of size with galaxy luminosity is unfortunate because it is nearly

TABLE 6  
LINEAR SIZES\* OF H II REGIONS IN THE CALIBRATING GALAXIES

Galaxy	$\langle D_H \rangle_1$	$\langle D_C \rangle_1$	$\langle D_H, D_C \rangle_1$	$\langle D_H \rangle_3$	$\langle D_C \rangle_3$	$\langle D_H, D_C \rangle_3$	$L_C$	$M_{pg}$
LMC.....	455	231	343	324	125	224	III-IV	-17.86
SMC.....	221	60	141	155	20	87	IV-V	-16.42
M33.....	436	214	325	456	149	302	II-III	-18.49
NGC 6822.....	137	40	89	123	23	73	IV-V	-15.82
IC 1613.....	147	0	73	113	3	58	V	-14.55
NGC 2403.....	523	176	350	424	124	274	III	-19.00
NGC 2366.....	323	139	232	244	64	154	IV-V	-16.34
NGC 4236.....	444	113	279	381	75	228	IV	-17.53
IC 2574.....	265	88	176	211	52	132	IV-V	-16.69
Ho II.....	307	24	165	276	12	143	IV-V	-16.53
Ho I.....	202	19	110	165	13	89	V	-14.36

\* In parsecs.

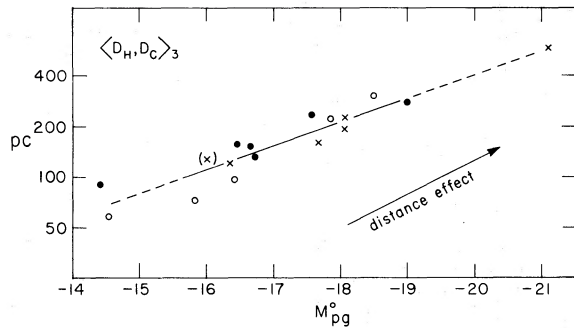


FIG. 9.—Correlation of the mean core-plus-halo diameters of the first three largest H II regions with absorption-free absolute blue magnitudes for the 17 calibrating galaxies. *Open circles*, members of the Local Group; *closed circles*, members of the M81-NGC 2403 group; *crosses*, members of the M101 group. The effect of arbitrarily increasing the distances to the galaxies is shown by the arrow.

the “null” solution of slope  $-0.2$  where the angular size of H II regions of nearby dwarf galaxies would be identical with those in distant galaxies of the same apparent magnitude. Without independent knowledge of  $M_{pg}^0$  we cannot enter the calibration curve of figure 9 properly even for the first time for a normal iteration procedure. With successive iterations from an assumed first guess, one moves up or down the “distance effect” line. And since it is the intersection of this line

with the correlation line that admits convergence of the iteration, the method in this form is clearly useless as a distance indicator because the lines intersect so shallowly.

Some modification of figure 9 is therefore necessary such that knowledge of  $M_{pg}$  is not required a priori. The natural choice for a replacement variable is the van den Bergh luminosity class,  $L_C$ , which can be determined by inspection of well-exposed large-scale photographs, and is distance independent.

b) Calibration as a Function of Luminosity Class

The correlations of  $\langle D \rangle$  with  $L_C$  are shown in figures 10 and 11 for six combinations of core and halo diameters. Closed circles are galaxies in the Local and the M81-NGC 2403 groups. Again, crosses represent the M101 group. Least-squares solutions give

$$\langle D_H \rangle_1 = -137L_C + 877, \quad \sigma(\Delta D/D) = 0.24; \quad (2)$$

$$\langle D_C \rangle_1 = -87L_C + 458, \quad \sigma(\Delta D/D) = 0.59; \quad (3)$$

$$\langle D_H, D_C \rangle_1 = -112L_C + 668, \quad \sigma(\Delta D/D) = 0.25; \quad (4)$$

$$\langle D_H \rangle_3 = -133L_C + 807, \quad \sigma(\Delta D/D) = 0.23; \quad (5)$$

$$\langle D_C \rangle_3 = -60.5L_C + 309, \quad \sigma(\Delta D/D) = 0.63; \quad (6)$$

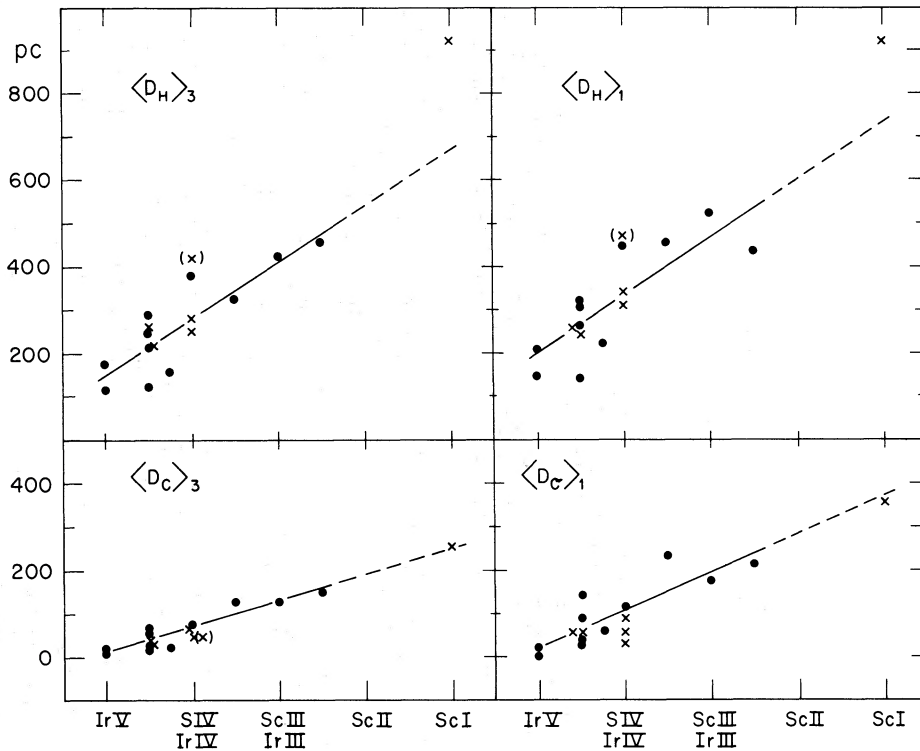


FIG. 10.—Correlation of various core and halo diameters with luminosity classes of the 17 calibrating galaxies. *Circles*, the Local and M81 groups; *crosses*, the M101 group.

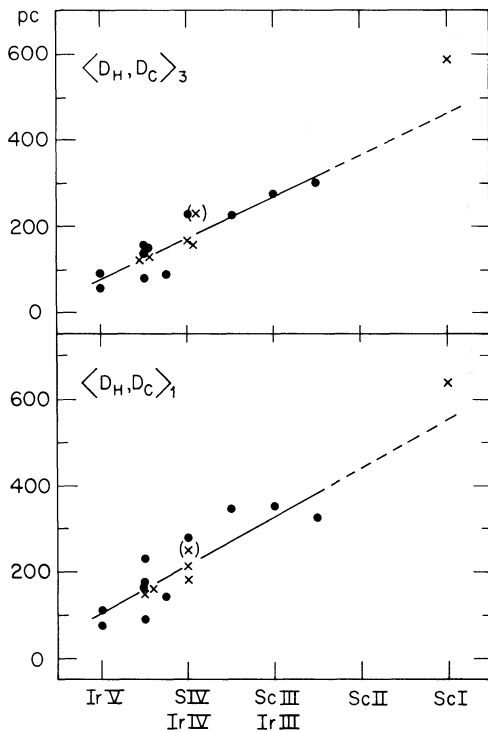


FIG. 11.—Same as fig. 10 for the mean core and halo diameters of the first and the first three largest H II regions.

and

$$\langle D_H, D_C \rangle_3 = -96.5 (\pm 14.4) L_C + 557 (\pm 60), \quad (7)$$

$$\sigma(\Delta D/D) = 0.24,$$

where  $L_C$  is the luminosity class, assigned numbers of 1, 1.5, 2, etc., for classes I, I-II, II, etc.

The M101 galaxies were not used in the solutions of equations (2)–(7), but it is evident from the approximate agreement of M101 itself (the single cross at Sc I) with the lines in figures 10 and 11 that the equations hold over the entire range of luminosity classes. We shall adopt the linear relations as the primary calibration on the basis of arguments in Paper IV which show that the H II regions in M101 are truly abnormally large, as given, in fact, in figures 10 and 11; i.e., we do not believe that the true relation curves upward at Sc I. This seems reasonable to us on the independent grounds that M101's H II regions do appear more conspicuous than the H II regions in other comparable galaxies.<sup>4</sup> This is especially true of the outlying region NGC 5471 which has been catalogued as a separate galaxy on many occasions.

#### c) Errors Due to Discrete Luminosity Classes

It should be noted that the mean percentage deviations ( $1\sigma$  values) quoted for equations (2)–(7) are

<sup>4</sup> Note in particular that the deviation ( $\Delta D/D = 0.21$ ) of the M101 point from the linear relation of figure 11 for  $\langle D_H, D_C \rangle_3$  lies in fact within less than  $1\sigma$  of the relation given by equation (7) where  $\sigma(\Delta D/D) = 0.24$ .

TABLE 7

MEAN ERRORS OF THE RELATIVE SIZES  $\Delta D/D$  OF H II REGIONS DUE TO THE WIDTH OF HALF-STEP LUMINOSITY CLASSES

TYPE OF DIAMETER	LUMINOSITY CLASS				
	I	II	III	IV	V
$\langle D_H \rangle_1$ .....	0.06	0.08	0.10	0.14	0.24
$\langle D_C \rangle_1$ .....	0.08	0.10	0.15	0.26	1.26
$\langle D_H, D_C \rangle_1$ .....	0.07	0.08	0.11	0.17	0.35
$\langle D_H \rangle_3$ .....	0.07	0.08	0.11	0.16	0.31
$\langle D_C \rangle_3$ .....	0.08	0.11	0.16	0.30	2.54
$\langle D_H, D_C \rangle_3$ .....	0.07	0.09	0.12	0.19	0.43

larger than expected from the observational errors discussed in the last section (table 5 and § IV), and larger than  $\sigma(\Delta D/D)$  of equation (1) from figure 9. Because the scatter of figure 9 is nearly independent of error in  $M_{pg}^0$  (due to the slope of nearly  $-0.2$ ), we believe that most of the additional scatter in figures 10 and 11 is due to the artificial discretization of galaxies into luminosity classes, rather than true cosmic scatter. Even if no error were to exist in our assignment of half-step luminosity classes to the galaxies, the width of each half-step in  $\sigma(M_{pg})$  introduces mean errors in the computed H II region sizes that are a large percentage error for luminosity class V galaxies. The discretization error, however, decreases as one proceeds toward luminosity class I galaxies.

The result of calculation of this artificial increase in the scatter (using the slope coefficients of eqs. [2]–[7]) are given in table 7, which shows that most of the increase of  $\sigma(\Delta D/D)$  can be explained in this way.<sup>5</sup>

#### d) Other Considerations

We note that the small galaxies in the Local Group SMC, NGC 6822, and IC 1613) lie systematically below similar galaxies in the M81 group in figures 10 and 11. It might be argued that this indicates an overestimate of our adopted distance to the M81 group. However, the same systematic deviation occurs in figure 9 where it could be reduced only by an unreasonably large change in distance. The effect is neither large nor significant within the errors of the calibration. The difference between the six galaxies in the NGC 2403 group and those in the Local Group is  $\langle \Delta \log D \rangle = 0.169$ , which is only a  $1.5\sigma$  effect. To make the regions identical in size would require  $(m - M)_0 = 26.71$  for the NGC 2403 group [ $\Delta(m - M) = 0.85$  mag]. We consider this change of distance to be unreal because the brightest-star criterion calibrated in Paper II gives no such effect. From the discussion given there (Paper II, § V), we conclude that the effect is statistical, and does not affect the calibrations in later papers of this series.

We note finally that the sizes of H II regions in all

<sup>5</sup> It is evident from the size of  $\sigma(\Delta D/D)$  in equations (2)–(7) compared with the quoted errors in table 5 that our measuring errors (§ IVa) have a negligible effect on the scatter in figures 10 and 11.

galaxies in our sample, even the dwarfs, exceed the largest optical H II regions known in the Galaxy. The halo and core of the Orion Nebula appear on the *Palomar Sky Survey* under angles of  $\sim 12''.8$  and  $1''.3$ , respectively, corresponding to  $D_H \simeq 110$  pc and  $D_C \simeq 11$  pc if the distance is 500 pc. The outer extension of the  $\eta$  Car nebula measures  $4^\circ \times 4^\circ$  on the Stromlo H $\alpha$  Atlas (Rodgers *et al.* 1960); this corresponds to a diameter of  $D_H \simeq 150$  pc at a distance of 2.2 kpc (Sher 1965). It is not known if the small size of the Galactic optical H II regions is a systematic selection effect or if it is real, possibly indicating an earlier type for the Galaxy.

## VI. CONCLUSIONS

1. The linear sizes of the largest H II regions in late-type galaxies increase with the luminosity of the parent galaxy.
2. The increase has a slope of  $\Delta \log D / \Delta M_{pg} = -0.14$ , which is so close to the distance independent value of  $-0.2$  as to make straightforward use of H II regions as distance indicators impossible. Two galaxies with the same angular size for their H II regions are not, in general, at the same distance.
3. Calibration of  $\langle D \rangle = f(\text{luminosity})$  in terms of

van den Bergh luminosity classes circumvents the difficulty (figs. 10 and 11). Figure 11 is our final calibration.

The mean size of the largest H II regions varies from  $\langle D_H, D_C \rangle_1 \simeq 110$  pc for luminosity class V galaxies to  $\langle D_H, D_C \rangle \simeq 550$  pc for Sc I systems.

4. The percentage errors  $\Delta D/D$  are artificially enlarged over their cosmic values due to discretization of the luminosity classes. In our calibration, this error increases as one proceeds from Sc I galaxies toward lower luminosities. Hence distances will be less accurately determined for intrinsically faint galaxies than for bright, using the present calibration method.

It is a pleasure to thank Gary Tuton and Juan Carrasco, night assistants at the Hale telescope, for their cheerful help during the long course of this investigation. The photo lab was especially useful in the preparation of figures 2–8 for publication. We wish to thank Felice Woodworth for her customary excellent preparation of the diagrams for press, and Raquel Ferrer for preparing a difficult manuscript.

This and the following papers of this series were made possible by a National Science Foundation grant GP-14801 for two years during the analysis, and we are very grateful for this support.

## APPENDIX

### CORRECTIONS TO MEASURED ANGULAR DIAMETERS FOR STANDARD CONDITIONS

#### I. INTRODUCTION

It is necessary to investigate the effect on the measurements of various changes in the observational conditions so as to reduce all data to a standard condition.

Six effects were studied: (1) the effect of *different exposure times* on the angular sizes measured on 200-inch plates taken with RG1 or RG2 filters; (2) the exposure effect for 200-inch H $\alpha$  interference plates; (3) the difference between the broad-band RG and the narrow-band H $\alpha$  200-inch plates; (4) exposure-time effects for the electrostatic image-tube plates; (5) comparison of the image-tube data with the unaided 200-inch RG and H $\alpha$  direct series; and (6) comparison of 103aO (blue) plate data with the H $\alpha$  material. Equations are derived here for the six comparisons to correct all measurements to standard conditions of 200-inch *direct H $\alpha$  interference* plates.

#### II. EXPOSURE EFFECT FOR 200-INCH DIRECT PLATES TAKEN WITH A BROAD-BAND RED FILTER

Five 103aE plates with RG1 or RG2 filters with exposure times from 35 min to 120 min are available for NGC 2403 (table 3). Four such plates are available for M101 (listed in the forthcoming Paper III of this series) with an exposure range of 82–120 minutes. The data are listed in table A1 for the mean major- and

minor-axis diameters of the first three ranked regions in NGC 2403, and for the first four regions in M101 (the largest is not present on the 82-min exposure which has a displaced center).

Inspection of the table shows that there is no evident change of image size with exposure time for the *halo* boundaries. A change in *core* radius is suggested by the NGC 2403 data, but not by those for M101. Furthermore, the differences between plates of the *same* exposure time (the 120-min series) are of the same order as differences between plates of extreme exposure times, showing that there is no pronounced exposure-time effect in the present material.

This ideal situation suggests that the boundaries of H II regions are generally limited by physical conditions in the nebulae, rather than by the method of detection at the telescope.

The scatter that is present in table A1 can be attributed to the interaction of the photographic images of the H II regions with the spiral-arm stellar background of the parent galaxy. This will be a variable function of position of the H II region within the galaxy, the seeing conditions, and the speed of the emulsion. The very small exposure corrections which could formally be derived from table A1 would have no meaning because of these interaction effects. What is clear is that the exposure-time effects with RG filters are very small, if present at all, and have therefore been neglected.

TABLE A1  
CORE AND HALO SIZES FOR H II REGIONS IN NGC 2403 AND M101 ON 103aE PLATES WITH RG FILTERS FOR  
DIFFERENT EXPOSURE TIMES

## A. NGC 2403

EXPOSURE TIME (minutes)	LARGEST		SECOND		THIRD		MEAN	
	Halo	Core	Halo	Core	Halo	Core	Halo	Core
35.....	36.5	14.4	28.8	5.5	22.7	6.1	29.3	8.7
60.....	...	...	28.8	6.1	22.2	6.1	...	...
90.....	35.4	14.4	29.9	8.3	25.4	10.0	30.2	10.9
120.....	38.7	13.3	28.8	8.3	25.4	9.4	31.0	10.3
120.....	36.5	14.4	28.8	10.6	24.3	11.7	29.9	12.2

## B. M101

EXPOSURE TIME (minutes)	LARGEST		SECOND		THIRD		FOURTH		MEAN (II, III, IV)	
	Halo	Core	Halo	Core	Halo	Core	Halo	Core	Halo	Core
82.....	...	...	34.3	6.6	22.7	10.5	21.6	8.3	26.2	8.5
107.....	34.8:	13.8:	44.2	6.6	24.3	11.1	25.4	7.7	31.3	8.5
120.....	24.9	13.3	45.3	5.5	23.8	10.5	19.9	7.7	29.7	7.9
120.....	33.2	13.3	44.2	5.5	24.3	9.4	25.4	8.3	31.3	7.7

III. EXPOSURE-TIME EFFECT FOR 200-INCH H $\alpha$   
INTERFERENCE FILTER PLATES

There is insufficient duplicate material in table 3 on given galaxies to formally evaluate the effect for interference-filter data, as for RG plates. However, because the bandwidth is so narrow, the suppression of the background is more complete with the H $\alpha$  filter than with the RG colored glass, and the null result of the last section should be even more complete.

No exposure correction has been applied to the 103aE+H $\alpha$  filter plates in table 3. But even so, the point is unimportant here because all such 200-inch plates in table 3 have nearly equal exposure times

near 120 minutes, and a negligible correction would have been made in any case.

IV. COMPARISON OF BROAD-BAND RG AND  
NARROW-BAND H $\alpha$  DATA

H II regions are generally well separated from the background on the H $\alpha$  interference-filter plates, but it is to be expected that their measured sizes on red plates (103aE+RG filter) will be systematically larger as affected by the stellar background.

The effect can be evaluated in those cases where both types of plates are available for the same galaxy. Four galaxies exist with such plates in the present material, and the data are listed in table A2.

TABLE A2  
COMPARISON OF H II REGION SIZES ON PLATES TAKEN WITH BROAD-BAND RG FILTERS AND THE 80 Å (HW) INTERFERENCE FILTER

GALAXY	FILTER	FIRST		SECOND		THIRD		MEAN (I, II, III)	
		Halo	Core	Halo	Core	Halo	Core	Halo	Core
NGC 2403.....	RG*	36.8	14.1	29.0	7.8	24.0	8.7		
	H $\alpha$	36.5	13.3	31.5	7.7	19.9	6.1		
	H $\alpha$ /RG	0.992	0.943	1.086	0.987	0.829	0.701	0.969	0.877
M101.....	RG†	23.8	10.4	23.1	8.1	42.0	6.1	±0.075	±0.089
	H $\alpha$	22.7	7.7	18.8	7.2	23.2	2.8		
	H $\alpha$ /RG	0.954	0.740	0.814	0.889	0.552	0.459	0.773	0.696
NGC 628.....	RG	13.3	1.1	8.9	3.6	5.5	2.5	±0.118	±0.126
	H $\alpha$	10.0	0.6	7.8	2.2	5.8	2.2		
	H $\alpha$ /RG	0.752	0.545	0.876	0.611	1.055	0.880	0.894	0.679
NGC 1058.....	RG	3.9	2.2	5.3	1.7	3.1	1.1	±0.088	±0.102
	H $\alpha$	3.6	2.0	2.1	1.4	2.6	0.6		
	H $\alpha$ /RG	0.923	0.909	(0.396)	0.826	0.839	0.545	0.719:	0.760
Mean.....							±0.163	±0.110	
								0.879	0.753
								±0.045	±0.052

\* Measurements are the mean of five plates.

† Measurements are the mean of four plates: data are for regions II, III, and IV since No. 1 is near plate edge.

Analysis indicates a marginal effect for the halo measurements (slightly more than a  $2\sigma$  signal), and a larger effect for the core (a  $5\sigma$  effect). The data require that corrections be made to the RG data of the form

$$\text{Halo: } \theta_{H\alpha} = (0.88 \pm 0.05)\theta_{RG}, \quad (\text{A1})$$

$$\text{Core: } \theta_{H\alpha} = (0.75 \pm 0.05)\theta_{RG}, \quad (\text{A2})$$

to reduce it to the system of the fully exposed  $H\alpha$  plates.

We have generally corrected our measurements here and in the later papers of the series by equations (A1) and (A2) to the  $H\alpha$  system. However, in some well-resolved nearby galaxies (LMC, SMC, NGC 6822, and IC 1613) the  $H\text{ II}$  regions are so well defined and their extension so well traceable that we have adopted the uncorrected measurements as their true dimensions.

V. EXPOSURE-TIME EFFECTS FOR THE 200-INCH IMAGE-TUBE PLATES

Many of the galaxies in the extended problem (Paper IV) have plates taken with an S20 electrostatic image tube with  $H\alpha$  interference filter, photographed with baked IIaD emulsion pressed against an output-fiber-optic plate. We took a series of exposures on several galaxies specifically to evaluate the exposure effect for the image-tube plates.

The data, taken from later papers of the series, are listed in table A3. The time ratio  $\Delta t/t_0$  in column (3)

TABLE A3

EXPOSURE-TIME EFFECT ON CORE AND HALO SIZES FOR PLATES TAKEN WITH AN ELECTROSTATIC IMAGE TUBE AND INTERFERENCE FILTER

Galaxy	Exposure Time (min)	$\Delta t/t_0$	$\langle \text{Halo} \rangle$	$\langle \text{Core} \rangle$
Ho I.....	15	0	13.45	1.57
	7	-0.53	11.67	0.73
Ho IV.....	25	+0.67	7.87	1.58
	15	0	7.58	1.23
NGC 5474.....	7	-0.53	...	1.02
	15	0	13.47	2.03
NGC 5477.....	7	-0.53	11.72:	1.40
	15	0	7.17	1.65
NGC 5486.....	7	-0.53	6.60	0.83
	15	0	4.77	2.13
NGC 3486.....	7	-0.53	4.58	1.87
	15	0	7.73	2.40
NGC 3810.....	7	-0.53	6.60	2.03
	15	0	10.05	3.62
NGC 4214.....	7	-0.53	9.38	2.50
	20	+0.33	13.63	5.88
NGC 4395.....	7	-0.53	12.17	4.78
	20	+0.33	20.12	3.22
NGC 5068.....	7	-0.53	19.20	2.02
	20	+0.33	10.12	5.33
NGC 6015.....	7	-0.53	8.73	3.85
	30	+1.00	5.33	2.48
NGC 7741.....	12	-0.20	3.87	1.20
	15	0	4.15	2.33
	7	-0.53	3.48	1.85

NOTE.—The angular sizes are for the mean of the first three ranked  $H\text{ II}$  regions.

is the difference between the given exposure and the adopted standard exposure  $t_0$  (15 minutes), divided by  $t_0$ . Inspection of the entries shows that there is an effect, although small, in the expected sense that shorter-exposure plates show smaller angular diameters. The effect is clearly much less steep than a linear relation, and in the absence of more optimally spaced exposure ratios, we make the natural assumption that the apparent angular growth per relative time interval is proportional to the angular size of the region, i.e.,

$$\theta_0 = \theta_t e^{-k\Delta t/t_0}, \quad (\text{A3})$$

where  $\theta_0$  is the angular size for a standard exposure time  $t_0$ ,  $\theta_t$  the angular size for an exposure of  $t$ , and  $\Delta t \equiv t - t_0$ .

Least-squares solution for  $k$  using the data of table 3A gives

$$\text{Halo: } k = 0.192 \pm 0.026, \quad (\text{A4})$$

$$\text{Core: } k = 0.56 \pm 0.10,$$

where the errors are rms (i.e.,  $1\sigma$  values). The value of  $k$  for the halo shows the exposure effect to be small, in agreement with the analysis of § II of this Appendix. An exposure ratio of a factor of 2 (7.5 min to 15 min) produces only a ratio  $\langle \theta_0/\theta_t \rangle = 1.10$ , which is almost negligible. The effect is large for the core diameters, giving  $\langle \theta_0/\theta_t \rangle = 1.32$  for the same times, but the core enters with less weight than the halo in the adopted definition of the mean diameter (§ IIb).

VI. SYSTEMATIC DIFFERENCES BETWEEN DIRECT AND IMAGE-TUBE PLATES TAKEN WITH THE 200-INCH

The modulation transfer function is different for photographic plates and for image-tube photographs. This will introduce differences in the appearance of the wings of  $H\text{ II}$  regions on the available respective gray scales of each device; hence eye estimates of the diameters are expected to differ between data taken with each.

Plates are available for three galaxies taken with both methods. Measurements in the broad-band (RG) series were corrected to the  $H\alpha$  system by equations (A1) and (A2), and the image-tube data were corrected to  $t_0 = 15$  minutes by equation (A3). These normalized values are listed in table A4, from which it can be derived that

$$\text{Halo: } \theta_{H\alpha} = (0.84 \pm 0.04)\theta_{IT}, \quad (\text{A5})$$

$$\text{Core: } \theta_{H\alpha} = (0.66 \pm 0.03)\theta_{IT}, \quad (\text{A6})$$

as rather uncertain corrections. More data are needed to strengthen the determination. But again, the halo has by far the highest weight in the determination of the mean diameter because it is much larger than the core; hence the crucial coefficient is 0.84 for the halo. This is close enough to 1.0 that the error in distance from angular sizes due to uncertainties in the coefficient will be, at the most, 16 percent (assuming the

TABLE A4  
COMPARISON OF NORMALIZED ANGULAR SIZES ON DIRECT PLATES AND ON IMAGE-TUBE PLATES

GALAXY	PLATE	FIRST		SECOND		THIRD		MEAN (I, II, III)	
		Halo	Core	Halo	Core	Halo	Core	Halo	Core
NGC 672.....	IT	11".40	1".80	10".40	0".90	7".80	2".50	0.932	0.656
	H $\alpha$	10.65	1.10	9.50	0.25:	7.40	1.75		
	H $\alpha$ /IT	0.934	0.611	0.913	(0.3)	0.949	0.700		
NGC 4214.....	IT	16.35	11.90	15.20	1.65	7.80	3.50	0.749	0.664
	RG	14.60	9.10	10.25	0.80	5.30	2.60		
	H $\alpha$ /IT	0.893	0.765	0.674	0.485	0.679	0.743		
NGC 7741.....	IT	6.20	3.70	2.73	2.15	3.05	1.45	0.838	0.642
	RG	5.10	2.50	2.20	1.50	2.70	0.80		
	H $\alpha$ /IT	0.823	0.676	0.806	0.698	0.885	0.552		
Mean.....								0.840	0.655
								$\pm 0.035$	$\pm 0.034$

true value might, in fact, be 1.0). The true error is less, because an effect clearly does exist, as evidenced by the small rms error of equations (A5) and (A6) compared with the difference of the coefficients from 1.0.

#### VII. USE OF BLUE PLATES FOR MEASURING ANGULAR DIAMETERS OF H II REGIONS

Blue plates of galaxies are available in great numbers and are relatively fast to obtain. Hence, it is of interest to test if they are suitable for the present purpose. We have investigated 14 blue plates (103aO+GG13 or W2 filters) for seven different galaxies in the Local Group (NGC 6822) and the M81 group (NGC 2366, NGC 2403, NGC 4236, IC 2574, Ho I, and Ho II).

The first disappointment came from the fact that the independently selected largest H II regions in each galaxy coincide with those selected on H $\alpha$  plates in only 75 percent of the cases.

The second disappointment came from a comparison of the measurements from blue and H $\alpha$  plates. The comparison for halo and for core measurements is shown in figure 12, where the distribution of normalized differences in angle  $\Delta\theta/\langle\theta\rangle$  is plotted. Here  $\Delta\theta$  is the difference between the measurement on the blue plate and the mean diameter (previously defined in § IIb) of the three largest H II regions (obtained by averaging the H $\alpha$  data of table 4 of the text and the data for the blue plates). Measurements of the halo dimensions were taken over directly from the blue data, but core diameters needed a correction of  $\theta_{H\alpha} = 1.61\theta_{\text{blue}} - 2".24$  to reduce a systematic difference.

Figure 12 shows that the error distribution of halo diameters on blue plates has a sigma of 14 percent for a single measurement, which is only slightly larger than the 12 percent (§ IV) for H $\alpha$  plates. However, the rms error for core dimensions is 57 percent, which is much larger than the 18 percent for H $\alpha$  plates (§ IV). From this, it appears to be virtually impossible to derive useful core dimensions from blue plates. The

result can be understood as core contamination by the cluster of blue stars that lie at the centers of the H II regions. This fact, and the poor identifiability of H II regions on blue plates, has induced us to refrain from their use in the present program.

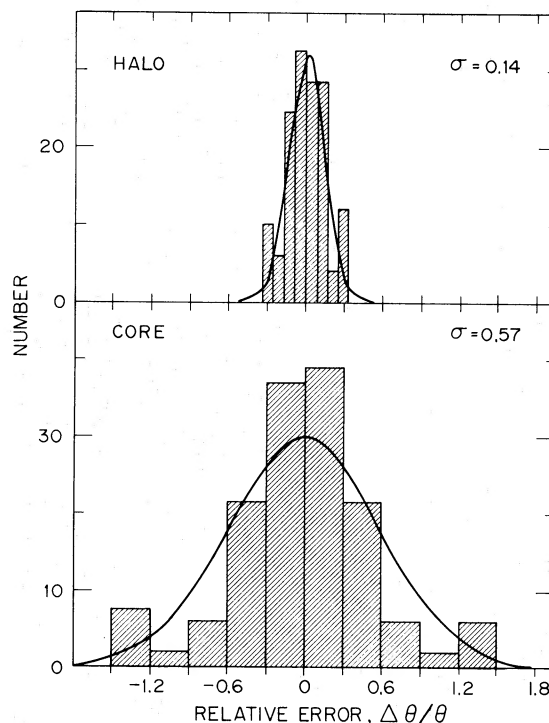


FIG. 12.—Distribution of differences of H II region diameters from measurements on blue and on H $\alpha$  plates of the same galaxies (8 cases). The sigma of the distribution of halo differences is of the same size as the measuring errors for single measurements on red plates, but the large sigma for blue-red differences for the core shows the very great difficulty of measuring blue core diameters.

## REFERENCES

- Baade, W. 1952, *Trans. IAU*, **8**, 397.  
 ———. 1956, *Pub. A.S.P.*, **68**, 5.  
 Carranza, G., Crillon, R., and Monnet, G. 1969, *Astr. and Ap.*, **1**, 479.  
 de Vaucouleurs, G. 1958, *A.J.*, **63**, 253.  
 ———. 1959, *Ap. J.*, **130**, 718.  
 ———. 1966, *Proc. Meeting on Cosmology for the Galileo Conference*, Vol. 2, Tomo 3, ed. L. Rosino (Florence: G. Barbera), p. 37.  
 de Vaucouleurs, G., and de Vaucouleurs, A. 1964, *Reference Catalogue of Bright Galaxies* (Austin: University of Texas Press).  
 Gascoigne, S. C. B. 1969, *M.N.R.A.S.*, **146**, 1.  
 Gum, C. S., and de Vaucouleurs, G. 1953, *Observatory*, **73**, 152.  
 Haggerty, M. J., and Wertz, J. R. 1971, *M.N.R.A.S.*, **155**, 495.  
 Henize, K. G. 1956, *Ap. J. Suppl.*, **2**, 315.  
 Hodge, P. W. 1966, *An Atlas and Catalog of H II Regions in Galaxies* (Seattle: University of Washington).  
 Holmberg, E. 1950, *Medd. Lund Astr. Obs.*, Ser. II, No. 128.  
 ———. 1957, *ibid.*, No. 136.  
 Hubble, E. P. 1936a, *Ap. J.*, **84**, 158.  
 ———. 1936b, *Ap. J.*, **84**, 270.  
 ———. 1936c, *The Realm of the Nebulae* (New Haven: Yale University Press; 1958 New York: Dover).  
 Hubble, E., and Humason, M. L. 1931, *Ap. J.*, **74**, 43.  
 Humason, M. L., Mayall, N. U., and Sandage, A. 1956, *A.J.*, **61**, 97.  
 Kayser, S. E. 1967, *A.J.*, **72**, 134.  
 McClure, R. D., and Racine, R. 1970, *A.J.*, **74**, 1000.  
 Purgathofer, A. Th. 1969, *Lowell Obs. Bull.*, **7**, 98.  
 Rodgers, A. W., Campbell, C. T., Whiteoak, J. B., Bailey, H. H., and Hunt, V. O. 1960, *An Atlas of H-Alpha Emission in the Southern Milky Way* (Canberra: Mount Stromlo).  
 Sandage, A. 1958, *Ap. J.*, **127**, 513.  
 ———. 1961, *ibid.*, **134**, 916.  
 ———. 1962a, *ibid.*, **136**, 319.  
 ———. 1962b, *Problems of Extragalactic Research, IAU Symposium No. 15*, ed. G. C. McVittie (New York: Macmillan).  
 ———. 1968, *Ap. J. (Letters)*, **152**, L149.  
 ———. 1971, *Ap. J.*, **166**, 13.  
 ———. 1972, *ibid.*, **178**, 1 (Paper II).  
 ———. 1973, *ibid.*, **183**, 711.  
 Sandage, A., and Hardy, E. 1973, *Ap. J.*, **183**, 743 (Paper VII).  
 Sandage, A., and Tammann, G. A. 1971, *Ap. J.*, **167**, 293.  
 ———. 1974, in preparation (Paper V).  
 Sandage, A., Tammann, G. A., and Hardy, E. 1972, *Ap. J.*, **172**, 253.  
 Seares, F. H., Kapteyn, J. C., and van Rhijn, P. J. 1930, *Mount Wilson Catalogue of Photographic Magnitudes in Selected Areas I-139* (Washington: Carnegie Institution of Washington).  
 Sersic, J. L. 1960, *Zs. f. Ap.*, **50**, 168.  
 Sher, D. 1965, *Quart. J.R.A.S.*, **6**, 299.  
 Stebbins, J., Whitford, A. E., and Johnson, H. L. 1950, *Ap. J.*, **112**, 469.  
 Strömgren, B. 1939, *Ap. J.*, **89**, 526.  
 Tammann, G. A. 1969, *Mitt. Astr. Ges.* No. 27, p. 55.  
 Tammann, G. A., and Sandage, A. 1968, *Ap. J.*, **151**, 825.  
 van den Bergh, S. 1960a, *Ap. J.*, **131**, 215.  
 ———. 1960b, *Zs. f. Ap.*, **49**, 198.  
 ———. 1960c, *Pub. David Dunlap Obs.*, **2**, No. 6.  
 ———. 1966, *A.J.*, **71**, 922.

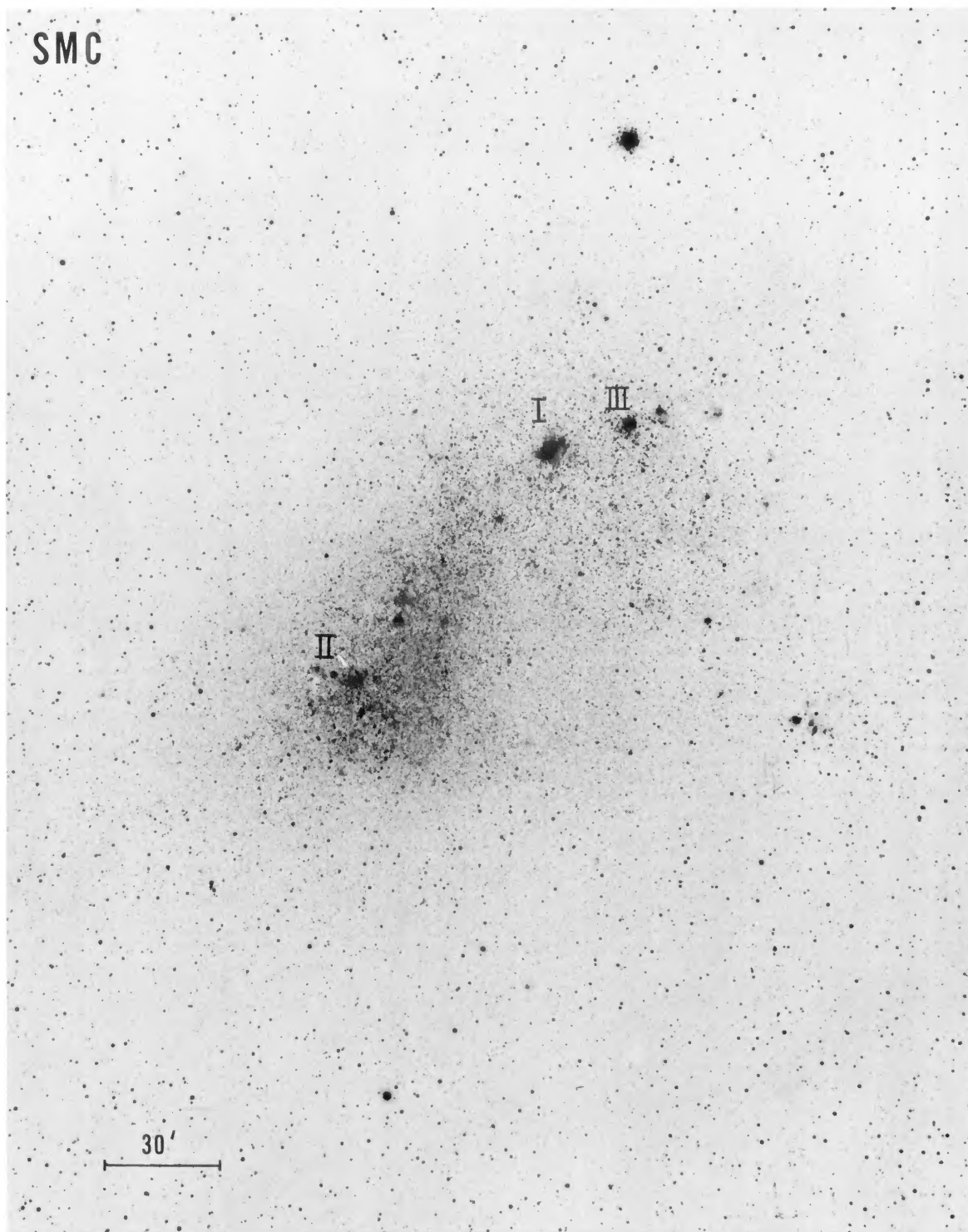


FIG. 2.—Broad-band red exposure of SMC taken by K. Henize with the Mount Wilson 25-cm refractor in South Africa. Eastman 103aE plus red Plexiglas filter of exposure time 300 minutes. North at top, west at right.

SANDAGE AND TAMMANN (*see page 527*)

PLATE 9

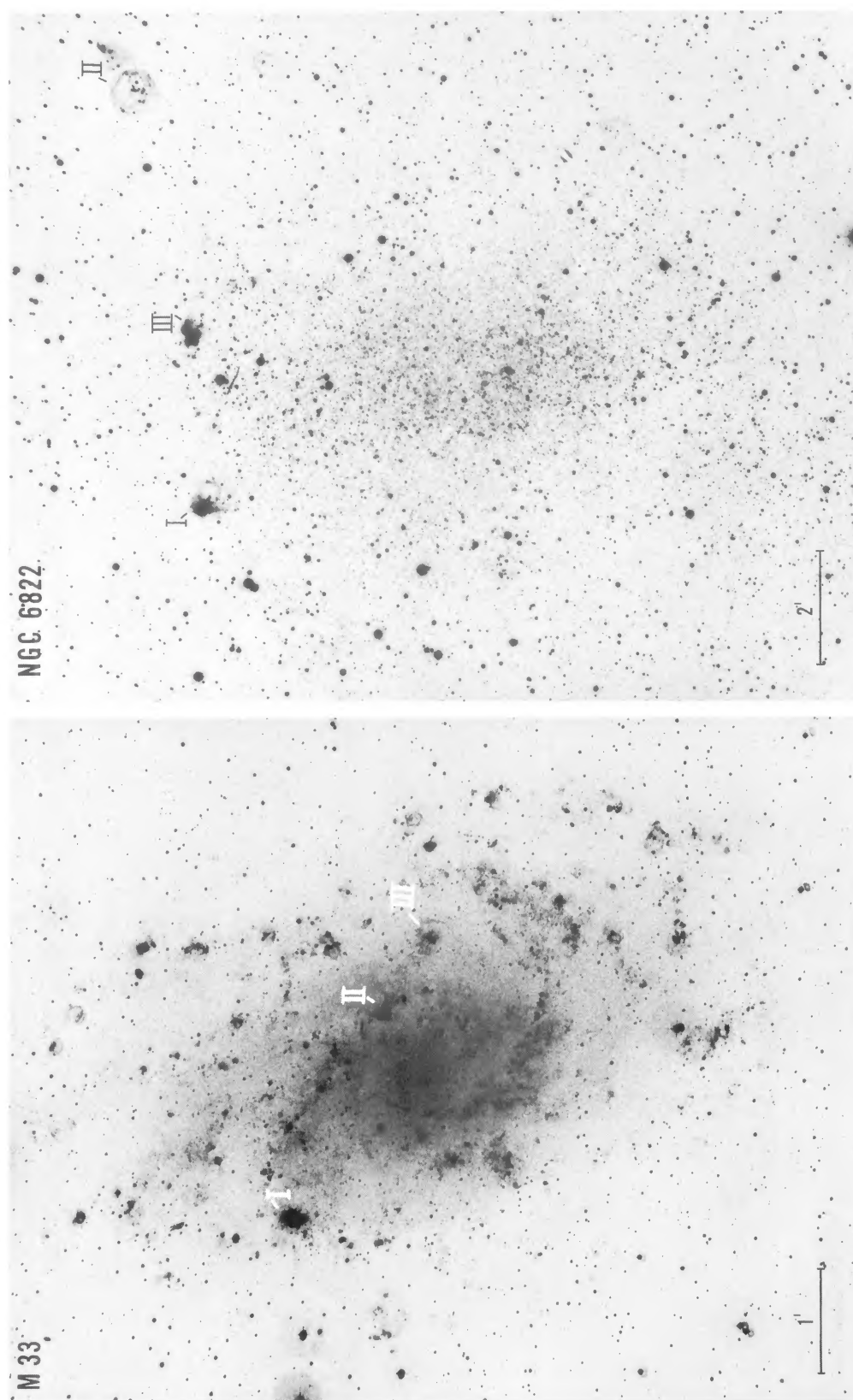


FIG. 3.—M33 from a Palomar 122-cm Schmidt plate taken with an H $\alpha$  interference filter with 180-minute exposure, compared with a copy of a paper print of Baade's broad-band (103aE + Wr. No. 25) plate of NGC 6822 taken with the Hale 5-m reflector with 80-minute exposure. North at top, west at right. SANDAGE AND TAMMANN (see page 527)

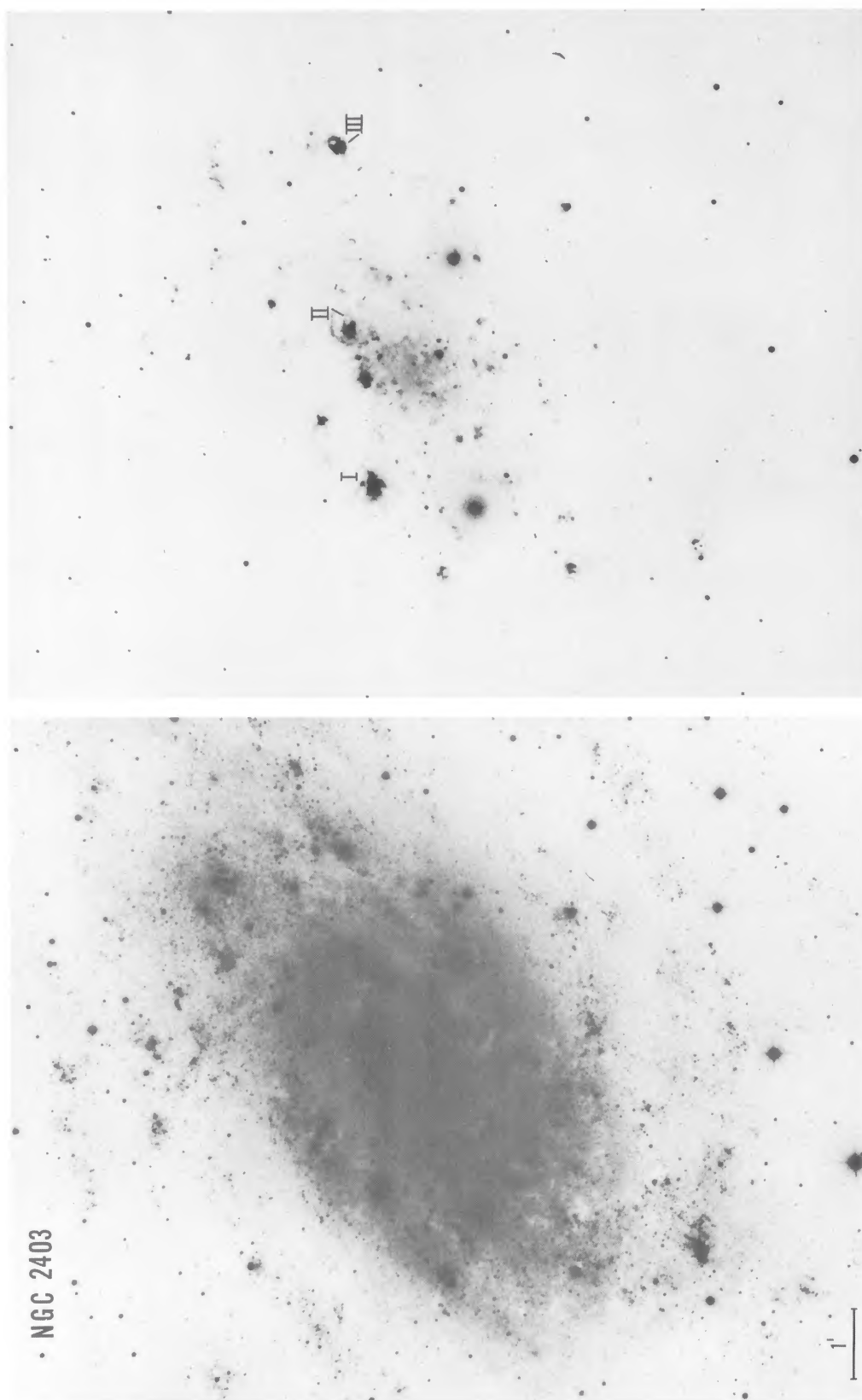


FIG. 4.—Comparison of a blue (103aO + GG1) and an H $\alpha$  exposure of NGC 2403 from plates taken with the Hale reflector. Exposure time 120 minutes for H $\alpha$ ; 30 minutes for blue. North at top, west at right.

SANDAGE AND TAMMANN (see page 527)

PLATE 11

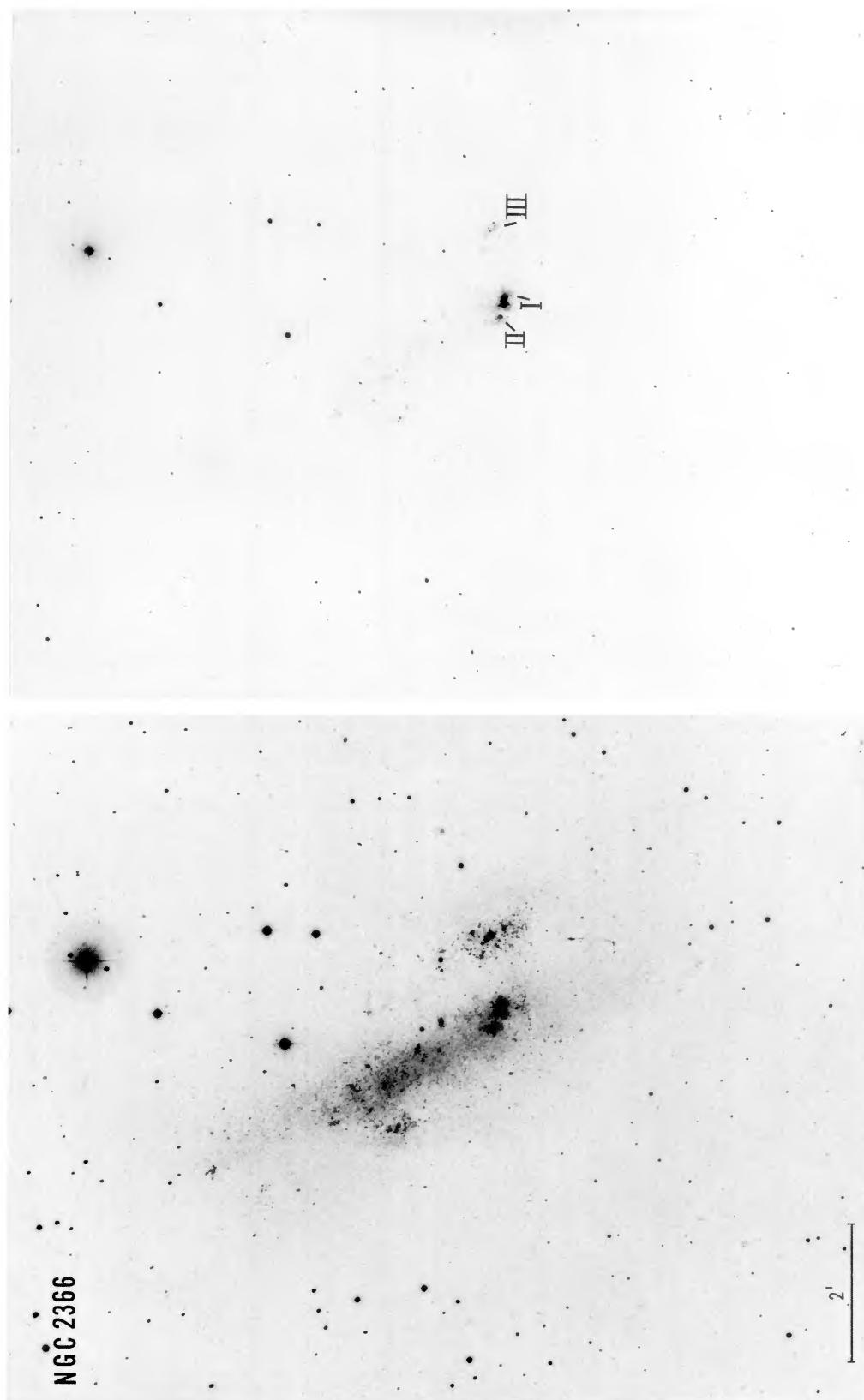


FIG. 5.—Broad-band blue (103aO + GG1) and H $\alpha$  plate for NGC 2366 with the Hale reflector. Exposure times are 30 and 110 minutes. North at top, west at right. SANDAGE AND TAMMANN (see page 527)

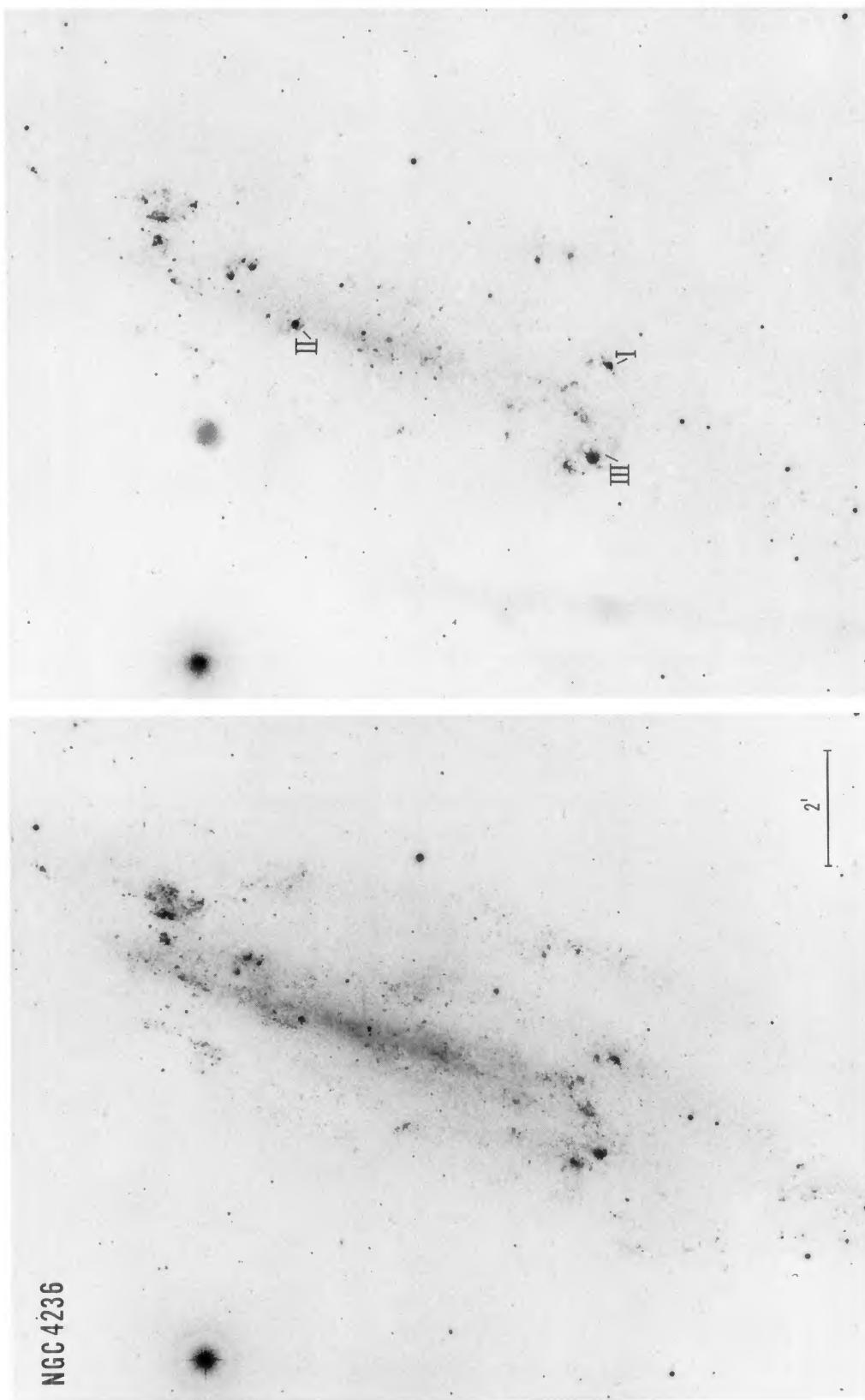


FIG. 6.—Broad-band blue (103aO) and H $\alpha$  plate for NGC 4236 taken with the Hale reflector. Exposure times are 20 and 120 minutes. North at top, west at right. SANDAGE AND TAMMANN (see page 527)

PLATE 13

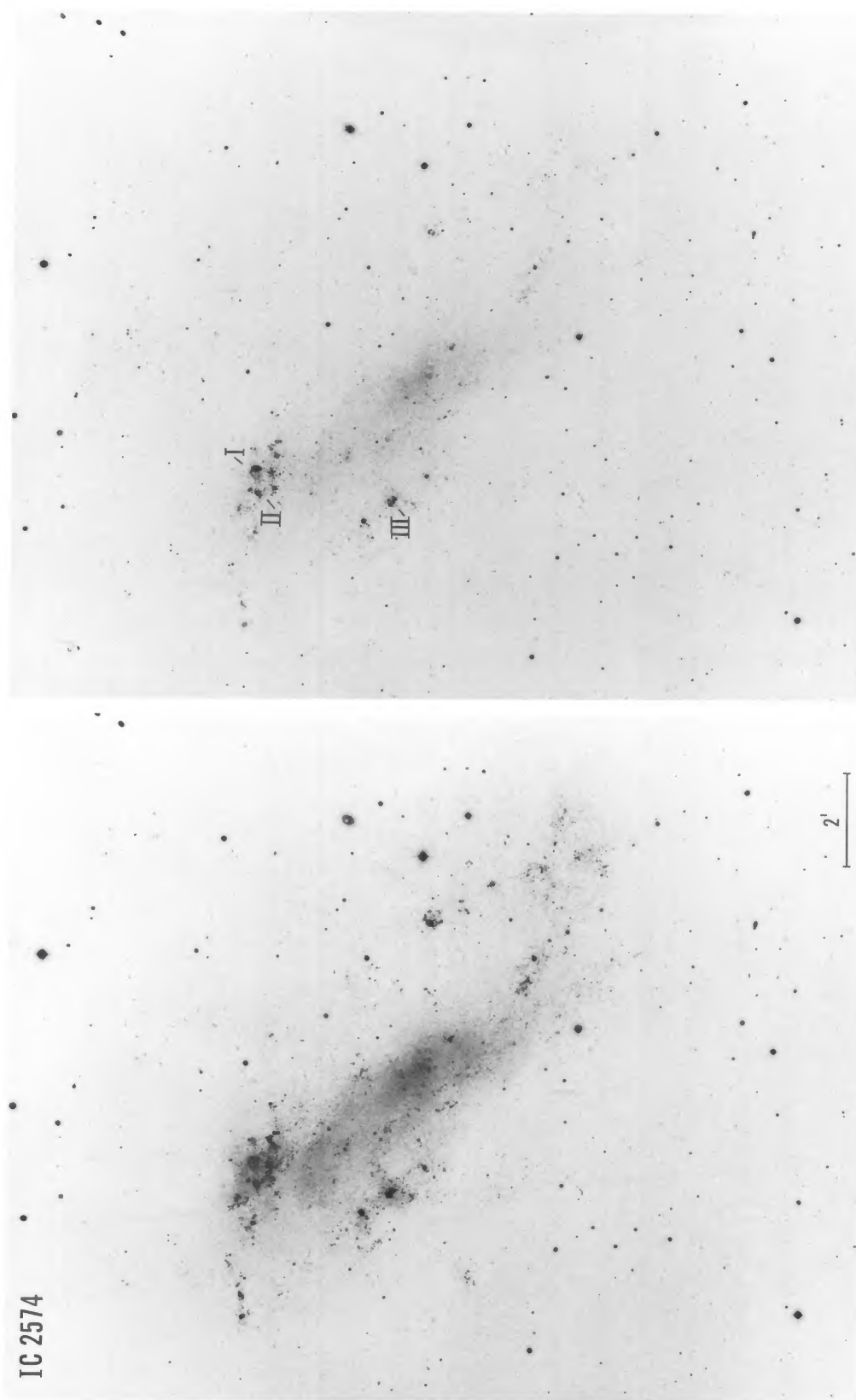


FIG. 7.—Broad-band blue (103aO + WG2) and red (103aE + RG1) plates of IC 2574 in the M81 group taken with the Hale reflector. Exposure times are 30 and 80 minutes. North at top, west at right. SANDAGE AND TAMMANN (see page 527)

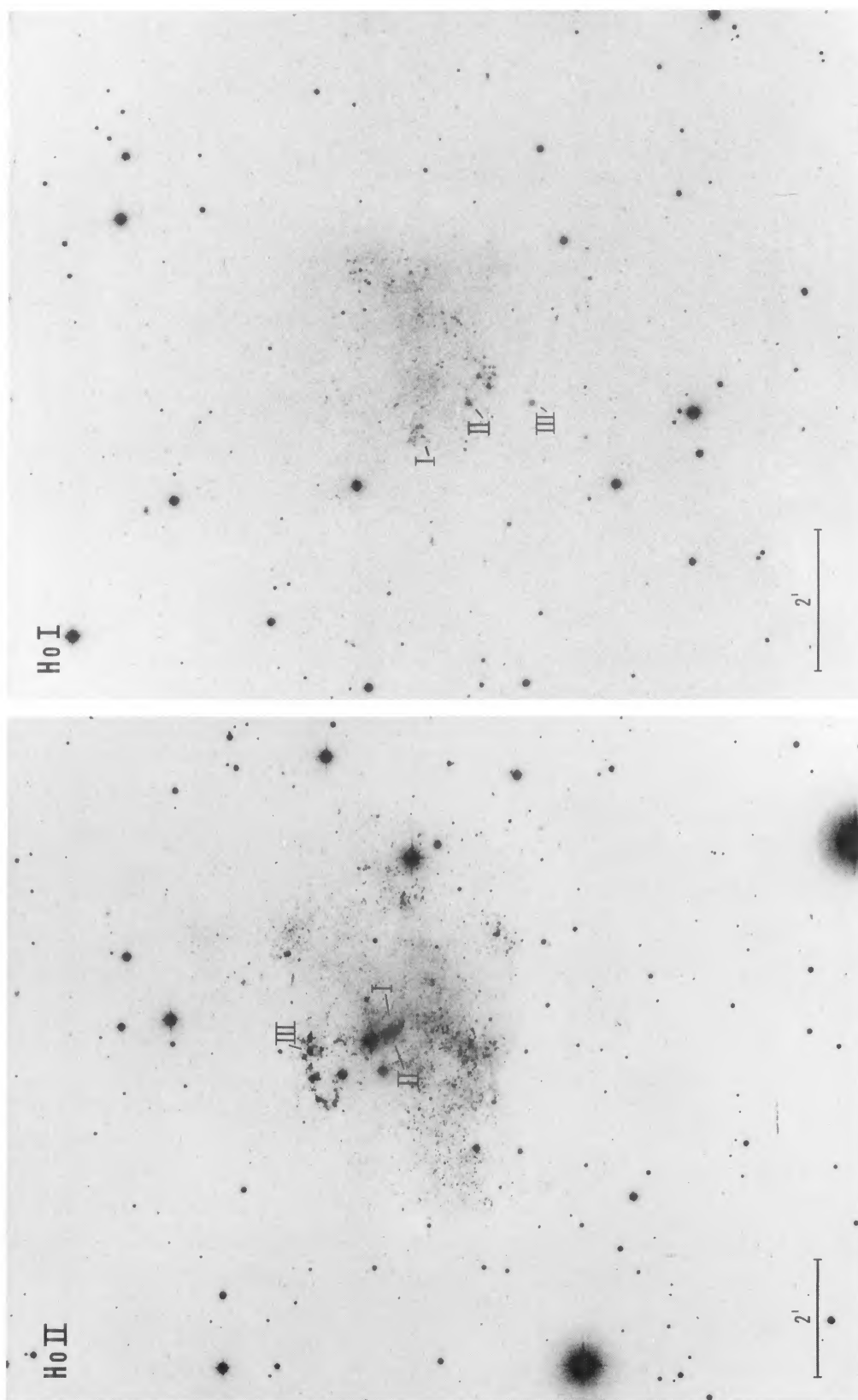


FIG. 8.—Broad-band blue plates of H $\alpha$  I and H $\alpha$  II taken with the Hale reflector with exposure times of 20 and 25 minutes, respectively  
SANDAGE AND TAMMANN (see page 527)